A spectral shaping approach to generate power vectors for optical ground-to-space links

Gianluca La Torre[a], Samuele Raffa[a], Juraj Poliak[a], Andrew P. Reeves[a], and Ilija Hristovski[a,b]

[a]Institute of Communications and Navigation, German Aerospace Center (DLR), Münchener Str. 20, 82234 Wessling, Germany

[b]School of Engineering, The University of British Columbia, 1137 Alumni Avenue, Kelowna, BC, Canada, V1V 1V7

ABSTRACT

Optical ground-to-space links (OGSL) are characterised by a highly dynamic channel, due to optical beam propagation through the atmospheric turbulence, leading to link power outages (also known as fades). The study of such stochastic fading process is an essential task to estimate the performance of OGSLs. The most common simulation methods used require an excessive computation time, hence are incompatible for network-wide simulations with a high number of possible links to simulate. A time-efficient alternative is provided by a random power vector generation approach which leverages on the knowledge of the power outages statistics and power spectral density (PSD). In this work, a modelling approach based on a Butterworth filter construction is presented as an effective solution to define the power outages PSD. The advantages of such method are displayed and the results are compared to OGSL simulation data obtained via a validated, alternative approach.

Keywords: Free-space optical communications, atmospheric turbulence, channel modelling, fades, power vectors, spectral shaping

1. INTRODUCTION

As the demand of the high-throughput satellite links increases, so does the necessity for efficient use of available resources, which, despite much higher available bandwidth and lower size, weight and power (SWaP), compared to the traditional RF-based satellite links, are becoming scarce.[1] With the onset of Terabit-per-second requirements,[2] the understanding of the system and channel modelling needs to be unified. This will not only improve the understanding of the available capacity, required SWaP and link margins, but also provide a unique reference, for instance, for the comparison of designed and implemented coding performance. System and sub-system designs and implementations need to reflect the channel model in order to avoid overdesigning — yielding high SWaP — but also underperforming — yielding low mission lifetime and impact. The iterative nature of developments as well as the increased performance demands, require models that are able to provide accurate results in seconds. This would allow to extend such models into operational systems to support routing in complex satellite (mega)constellations.

Previous works[3] which focused on the Low Earth Orbit (LEO) Direct-to-Earth (DTE) applications presented analytical models based on a spectral shaping method and reflected primarily the needs covered by the CCSDS O3K standard. The resulting reference power vectors were widely used and provided a strong basis for LEO downlink channel analysis. These, however, lack the inclusion of the impact of the adaptive optics and fibre-coupling on the signal statistics, as well as the description of the uplink channel. For more complex channel models, the phase screen method is widely used.[4] Its accuracy increases with the number and resolution of the phase screens, but at the cost of the computational effort. Hence, in the presented paper, the authors focus on the spectral shaping approach to generate power vectors, but assisted by the phase screen pre-analysis to derive the temporal performance of a bi-directional system. This method, as will be demonstrated, yields optimal

Correspondence:
Gianluca La Torre, Institute of Communications and Navigation, German Aerospace Center (DLR), Wessling, Germany
E-mail: gianluca.latorre@dlr.de

Environmental Effects on Light Propagation and Adaptive Systems VII, edited by Karin Stein, Szymon Gladysz, Proc. of SPIE Vol. 13194, 131940N

performance in terms of speed of calculations, accuracy and coverage of realistic system parameters. Moreover, it allows for a future, modular inclusion of the adaptive optics correction and fibre-coupling processes which occur at the optical ground station (OGS) system.

In the text we use the term of fade to describe a short-term (ms-level) loss of signal and its derivative term fading channel to distinguish it from e.g. AWGN-like channels observed in terrestrial fibre-optic or optical inter-satellite links and applications. The term power vector describes a vector of time-coherent samples of a relative loss of optical signal. The power vector can be, with the knowledge of system parameters such as required optical power, transmit power and transceiver performance, translated into vectors representing link margin development or erasure vector.

2. ATMOSPHERIC TURBULENT CHANNEL

When an optical signal propagates through the atmospheric medium, three main phenomena can be observed: absorption, scattering and refractive index fluctuations, i.e. turbulence. The first two processes are deterministic and cumulatively referred to as atmospheric attenuation.[5] For a given OGSL scenario they cause a static loss,[6] which can be included in the link budget calculation as a given margin in order to determine the absolute mean received power.

On the other hand, temperature fluctuations through a turbulent atmosphere cause random variations of the index of refraction (IR) of the medium. For an optical beam propagating through the atmosphere this effect induces random phase distortions of its wave-front, which, in combination with constructive and destructive interferences, lead to variations of the beam intensity in the beam profile. The dynamics of such fluctuations lead to short-term losses of the instantaneous received optical power, also referred to as fades.[4]

The IR can be modelled as a locally homogeneous and isotropic random field. Its statistical behaviour is represented by its structure function, which is defined by the structure constant C_n^2 ($[C_n^2] = \mathrm{m}^{-2/3}$). Past measurements have produced a variety of parametric models of C_n^2, describing it as a function of the beam height above ground h and including the effect of local ground conditions. The most common one, the Hufnagel-Valley (HV) profile,[4] is characterised, as can be seen in Eq. (1), by the two parameters A and w. These represent the value of the structure constant on ground and of the root mean square of the wind speed perpendicular to the line of sight, respectively.

$$C_n^2(h) = 0.00594(w/27)^2(10^{-5}h)^{10}\exp(-h/1000) + 2.7\cdot 10^{-16}\exp(-h/1500) + A\exp(-h/100) \tag{1}$$

The wind speed profile used to derive w can be modelled as a Bufton wind profile.[7]

$$V(h) = \omega_s h + v_G + 30\exp\Big[-\Big(\frac{h-9400}{4800}\Big)^2\Big] \tag{2}$$

As shown in Eq. (2), the wind speed $V(h)$ is given by the sum of an absolute wind component, which can be tuned through the parameter v_G describing the local wind speed on ground, and of a relative wind component caused by the satellite slew rate ω_s ($[\omega_s] = \mathrm{rad\ s^{-1}}$) with respect to the ground terminal. By including this apparent wind speed one can consider the effect of the space terminal kinematics on the propagating signal.

2.1 Asymmetric Downlink and Uplink Channels

The nature of the stochastic fading process experienced at the receiver of an OGSL depends on the link direction.

In both cases, the optical beam experiences scintillation, which is defined as the variance of the signal normalized by its square mean, and is completely described by the dimensionless scintillation index σ_I^2. Such process, due to the discussed wave-front distortions, presents itself on the receiver plane as a speckled pattern. This eventually results in efficiency degradation when the free-space laser is coupled into the receiver's fibre.[8] Because of the significantly different dimensions of the space and ground terminals compared to those of the received signal's coherence length, in combination with link asymmetry with reference to the propagation through the atmosphere, the scintillation index expressions for uplink and downlink yield different results.[9]

The uplink propagation channel is also characterised by a second random process known as beam wander. This is due to the optical properties of the atmospheric turbulent cells, and manifests itself as a random displacement of the optical beam with respect to its propagation axis. The process is entirely described by the parameter β,[10] which depends on the turbulence strength as well as on the transmitted beam divergence.

Whilst beam wander is the main contributor of the fades measured in the uplink channel, it does not represent a concern for the downlink. In fact, in this case the beam reaches the turbulent atmosphere towards the end of its path, where the wave-front is practically planar.

3. CHANNEL MODELLING

Channel modelling is required to estimate the signal losses suffered in an OGSL and to obtain a realistic time-series of the fades experienced at the receiver.

For this purpose, several approaches can be followed: the use of direct measurements, if available; the use of numerical electro-magnetic field propagative simulators, which model the turbulent atmosphere through a series of random phase screens; or the use of power vector generator tools based on analytically defined fading statistics.

3.1 Direct Measurements

Measurements of the OGSL turbulent channel can be performed by establishing links between two laser communication terminals based on ground and in space. The measurements are collected and during the data analysis the biases which are due to the particular communications system employed are removed where possible. This is required in order to decouple the channel effects on the signal from those due to the system, such as the disturbances introduced by the satellite reaction wheels or the fibre coupling loss which occurs after the light is collected from the receiving aperture.

A considerable amount of experiments and measurement campaigns of this type have been realized in the past decades, many of which by the DLR Institute of Communications and Navigation (DLR-KN).

Of great interest are the KIODO experiments carried out between 2006 and 2009[11–13] between the DLR-KN OGS and the OICETS LEO satellite, as well as the recent measurement campaign which took place between the DLR-KN OGS and the laser terminal on board the Alphasat geostationary (GEO) satellite.[14] In the first case, measurements of the received optical power and other key parameters, such as the Fried coherence length r_0 and the scintillation index σ_I^2, allowed the assessment of the turbulent downlink channel. The data analysis enabled also the refinement of the models used to describe the fades statistics and their frequency response. In the second case, bi-directional links were established both with and without the engagement of a ground-based adaptive optics (AO) system. Measurements of the received optical power for the two AO configurations allowed to investigate and quantify the mitigation effect of the adaptive optics on the quality of the received beam in GEO OGSLs.

Such measurement campaigns are of immense value since the data obtained can be analysed to assess real world optical turbulence. Nevertheless, the measurements are obviously descriptive of actual, fixed scenarios, hence it is not possible to directly implement the data into network simulators, where the countless OGSL configurations depend on a wide range of inputs. Instead, the direct measurements are used as a means to validate the proposed models at a given scenario, i.e. for a particular system realisation or for a given subset of input parameter values.

3.2 Phase Screen Simulations

When modelling the propagation of electromagnetic waves through the atmosphere, the "phase screen" method — or the concept of representing a volume of randomly fluctuating media through a minimal number of two-dimensional phase screens — has been used by researchers for decades.[15–19] It is particularly useful as it mitigates the computational burden of modelling a three-dimensional volume and still accounts for the effect that the randomly fluctuating media has on an electromagnetic wave that propagates through it with a reasonable accuracy. When implementing this method, the propagation direction is typically assumed to be perpendicular to the set of phase screens, and a series of Fresnel diffraction integrals is solved to model the interaction with and propagation between each phase screen.[15] This method has been used more recently in End-to-end Monte Carlo simulations for OGSLs that use adaptive optics for the correction of the atmospheric turbulence effects.[20, 21]

End-to-end Monte Carlo (E2EMC) simulations can offer significant advantages when designing and optimizing free space optical communications (FSOC) links or their system architectures, primarily due to their customizability and modularity. A highly modular E2EMC simulation was used in this work to simulate a bidirectional FSOC link. The simulation consists of various customizable modules that can be connected based on the desired FSOC link configuration. For example, the atmospheric module generates a series of large phase screens with von Kármán atmospheric turbulence statistics using a fast-Fourier transform based method.[22] Each phase screen is assigned an atmospheric turbulence strength, inner and outer scale, wind speed, and wind direction to allow for the simulation of specific atmospheric turbulence strength $C_n^2(h)$ and wind speed $V(h)$ profiles. The line-of-sight module then extracts smaller portions from each of these larger atmospheric phase screens depending on the FSOC link geometry, e.g. elevation and azimuth angles between the OGS and the satellite. The link module uses angular spectrum propagation — employing a specialized solution to the Fresnel diffraction integral at the desired wavelength — to simulate the propagation and diffraction effects between each atmospheric phase screen. In the uplink direction, a fast-Fourier transform is used to represent far-field (Fraunhofer) propagation from the highest atmospheric phase screen to the satellite. The aperture and satellite modules can be configured with the appropriate physical dimensions and used to extract the portion of light entering the apertures at the OGS and satellite, respectively.

For the FSOC link configuration used in this work, a plane wave is assumed to be entering the atmosphere due to the sufficiently far distance that the original transmitted beam diverges from the satellite to the top of the atmosphere. This plane wave is propagated down through the atmospheric phase screens and a portion of it enters the OGS telescope, where metrics such as the Strehl ratio, angle of arrival, and received power can be extracted. Two discrete modified Hufnagel-Valley (HV) turbulence strength profiles, $C_n^2(h)$, are used when generating the atmospheric phase screens, namely a "strong" turbulence profile (representing daytime link operation) and a "weak" turbulence profile (representing nighttime link operation). The Bufton wind model is also used when generating the atmosphere's wind profile. The atmosphere was chosen to be represented by seven atmospheric phase screens as this provided a good balance between minimizing the computational time for each propagation while maintaining accurate representations of the turbulence and wind speed profiles. Various elevation angles and satellite altitudes can also be configured. The relevant simulation parameters used for the results section are listed in Table 1. Example intensity and phase profiles received by the OGS telescope are depicted in Fig. 1.

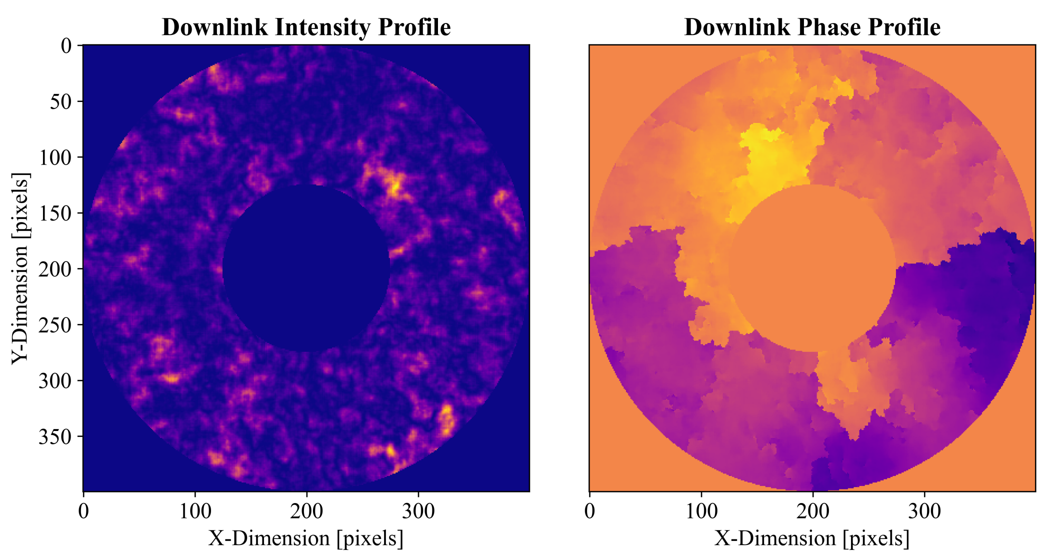

Figure 1: Representative downlink received intensity and phase profiles (from simulation).

Table 1: Relevant simulation parameters.

Parameter	Variable	Value	Unit
General Link Parameters			
Wavelength	λ	1550	nm
Simulation iteration rate	f	2, 4	kHz
Elevation angle	θ_{elev}	40	deg
OGS Parameters			
OGS altitude above mean sea level	h_{OGS}	602	m
Downlink telescope diam.	D_{Rx}	80	cm
Downlink central obscuration diam.	D_{cent}	30	cm
Uplink hard aperture diam.	D_{Tx}	25	cm
Uplink beam waist radius	ω_0	∼8.8	cm
Satellite Parameters			
Satellite altitudes (Zenith)	L	LEO: 1000 GEO: 35786	km
Satellite aperture diameter	D_{SAT}	LEO: 13.5 GEO: 25	cm
Atmospheric Parameters			
Number of phase screens	–	7	–
Atmospheric turbulence profile type	–	Modified HV	–

This method displays extraordinary advantages and can be used to assess the performance of OGSLs with virtually any configuration. It also allows for the testing of various mitigation techniques, such as adaptive optics or aperture averaging techniques. Despite this extreme versatility, this approach is still quite time consuming and thus not apt for network wide simulations.

3.3 Generation of Random Vectors with Desired Specifications

A third approach consists in artificially generating vectors which are representative of the received optical power in a turbulent ground-to-space link. This can be done by employing a random signal generation algorithm first presented in 1968 by Gujar and Kavanagh.[23] In this work, the authors present how one can exploit the statistics and the frequency response of a stochastic process in order to generate a synthetic realization which meets the input specifications with acceptable accuracy.

In order to obtain a realistic realization of a signal $y(t)$, with known statistics and spectrum $Y(f)$, one can firstly generate a Gaussian signal $x(t)$ with null mean and unitary variance. By definition, $x(t)$ is characterised by a constant spectrum. The second step consists in scaling the spectrum $X(f)$ by a function $H(f)$ such that the new spectrum $X'(f) = H(f)X(f)$ resembles that of the desired signal $y(t)$. Such spectral shaping process is required in order to impose the desired dynamics to the synthetic signal, and it is demonstrated how the filter $H(f)$ must be such that its modulus is equal to the square root of the desired signal's power spectral density (PSD):

$$|H(f)| = \sqrt{PSD_Y(f)} \tag{3}$$

Once the filtered signal is normalized with respect to the square root of its variance, a zero-memory non-linear transformation is applied in order to obtain a signal $z(t)$ which displays the desired probability density function (PDF).

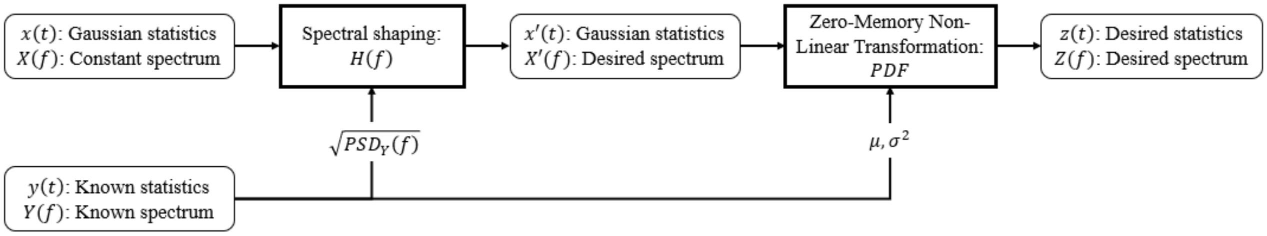

Figure 2: Visual representation of the random vector generation algorithm. A vector $z(t)$ with the desired statistics and spectrum of a vector $y(t)$ is generated from a Gaussian vector $x(t)$. In particular, the probability distribution function (PDF) of $z(t)$ is derived from the statistical parameters of $y(t)$.

The strength of such algorithm — condensed in Fig. 2 — resides in the fact that it conveniently enables the synthesis of one realization of a stochastic process starting from a Gaussian vector by simply knowing the process' PDF and PSD.

In the particular case of atmospheric turbulence, studies performed on OGSL measurements have yielded models which enable the analytic description of the fades' statistics.[24,25] Scintillation can be described as a log-normally distributed process, with mean and variance completely defined by the scintillation index. Beam wander, which scales the power fluctuation by a factor comprised between 0 and 1, is described by a beta distribution with mean and variance defined by the value of β. In the uplink channel model the joint statistics are derived by considering scintillation and beam wander as two independent processes.

This knowledge on turbulence statistics has enabled researchers at DLR-KN to develop a simulation tool — named PVGeT — able to output realistic time-series of the fading vectors.[3,26] Based on the stochastic vector generation principle described above, the convenience of such tool resides in the fact that it allows the fast derivation of realistic time-series of the fades experienced in OGSLs. Moreover, if the output vector is added to the mean received power which is easily obtained from the link budget computation, one is able to estimate the vector of the total received optical power for a given scenario.[27]

For details concerning the use of the fades' statistics in the PVGeT, the references pointed above are exhaustively explanatory. The implementation of the spectral shaping, on the other hand, lacks an accurate description. The goal of the present work is to clarify which PSDs describe the fading process and how to conveniently implement the spectral shaping in a vector generation tool in order to apply the atmospheric turbulence dynamics. In particular, rather than using experimentally derived filters obtained for discrete scenarios, the objective is to present a model to generate filters for variable OGSL conditions.

4. ATMOSPHERIC TURBULENCE SPECTRUM

The frequency response of the fading process measured at the receiver depends on the atmospheric turbulence dynamics. The expression which is often employed as a first approximation to analytically describe the atmospheric spectrum is given by the Kolmogorov model:[4]

$$\Phi(\kappa) = 0.033\, C_n^2\, \kappa^{-11/3} \tag{4}$$

with C_n^2 being the turbulence structure constant and κ the wave number. Eq. (4) is also referred to as the Kolmogorov power-law spectrum, and it holds its validity for the assumption of an infinite outer scale of turbulence L_0 and an infinitesimal inner scale of turbulence l_0. Other atmospheric spectrum analytical models are also available, however their application comes at a cost of considering a larger set of hypotheses.

In addition to the effect of the optical turbulence, the measured signal is also affected by the physical aperture at the OGSL receiver side. The impact such finite aperture has on the fades' spectrum needs to be included.

4.1 Analytic Zernike-Polynomials-Based Power Spectrum

The wave-front of the optical beam which is received by a circular aperture can be exactly described by an infinite set of Zernike polynomials. Those are orthogonal polynomials defined on a unit circle and constitute a convenient basis to describe the distortions sensed at the receiver.[28]

Each Zernike polynomial Z_n^m, or mode, is the product of a radial function and an angular function, and is described by the pair of indices n and m which define, respectively, the polynomial's radial degree and its azimuthal frequency. The increase of the radial degree corresponds to a higher resolution of the wave-front aberrations described by the Zernike polynomial. The first radial degree $n = 0$ corresponds to the piston mode, which identifies the mean phase offset and is constant for the whole unit circle; the radial degree $n = 1$ describes the tip-tilt of the received beam; and for $n > 1$ the Zernike polynomials describe wave-front aberrations of increasingly higher order.

The considerations developed in Sec. 2.1. concerning the random processes caused by atmospheric turbulence relate beam wander to the tip-tilt of the beam, and scintillation to the higher order wave-front distortions. Hence, it is possible to describe the dynamics of the beam wander measured on a circular aperture by those of the Zernike polynomials of radial degree $n = 1$, while the scintillation dynamics can be described by those of all the Zernike polynomials of higher radial degree. Even though the radial degrees are in theory infinite, it has been seen that the inclusion of the first 231 Zernike modes, i.e. until $n = 20$, is sufficient to accurately describe the scintillation process measured in an OGSL.[29]

By combining the frequency response of the atmospheric spectrum provided by the Kolmogorov power-law with that of the Zernike polynomials, it is possible to describe the frequency response of the OGSL beam wander and scintillation. Leveraging on the work presented by Conan[30] one can express, for each radial degree n, the PSD of the measured wave-front distortion as:

$$PSD_{Zern_n}(f) = \frac{12\,(n+1)}{(\pi D_{\mathrm{Rx}})^2}\, 0.033\,(2\pi)^{-2/3}\left(\frac{2\pi}{\lambda}\right)^2 \int\limits_h \frac{C_n^2(h)}{V(h)} \int\limits_x \frac{\left|J_{n+1}\left(\pi D_{\mathrm{Rx}}\sqrt{\left[\left(\frac{f}{V(h)}\right)^2 + x^2\right]}\right)\right|}{\left[\left(\frac{f}{V(h)}\right)^2 + x^2\right]^{17/6}}\, dx\, dh \qquad (5)$$

where λ is the signal wavelength ($[\lambda] = m$), $J_{n+1}(\cdot)$ is the Bessel function of first kind, D_{Rx} is the receiver diameter, x is the spatial frequency and f is the temporal frequency. In particular, Eq. (5) has been derived for a general ground-to-space link, for which the altitude h is considered a variable between the ground station altitude and that of the satellite.

The integration of Eq. (5) yields the power spectral density for each Zernike radial degree as a function of the temporal frequency f. As depicted in Fig. 3a, the curves' characteristic ripples are an effect of the Bessel function $J_{n+1}(\cdot)$. In order to describe the frequency response of the scintillation process in the downlink, one can then exploit the orthogonality of the Zernike polynomials and perform the summation of all the Zernike modes' PSDs with a radial degree $n > 1$. For the uplink, which is characterised also by the beam wander, one must also include the PSD of the Zernike modes representative of the tip-tilt, i.e. those of radial degree $n = 1$.

Such curves represent valid candidates for the analytic representation of the temporal power spectrum of the fading processes measured in both directions of OGSLs. Given the considerations on the filter which is required to perform spectral shaping (see Eq. (3)), one can then apply the square root to the PSDs. As shown in Fig. 3b, the filter's high frequencies are characterised by a common asymptote of $f^{-17/6}$, while the lower frequencies display a different behaviour according to the channel. The downlink filter follows a flat f^0 curve, while the contribution of the tip-tilt in the uplink introduces a $f^{-1/3}$ asymptote. In accordance with previous publications,[30] in both cases the cut-off frequencies are proportional to the ratio $V(h)/D_{\mathrm{Rx}}$, highlighting how the wind speed and the receiving aperture affect the frequency response. As clearly visible from the comparison of Fig. 3a with Fig. 3b one can notice how the truncation of the Zernike radial degrees at $n = 20$ in the PSD summation causes a slight divergence of the filter with respect to the $f^{-17/6}$ asymptote for very high frequencies. Nevertheless, the filter's gain in such spectral region is of at least 3 orders of magnitude lower than what is displayed before the characteristic cut-off frequencies, hence it is not a concern.

As mentioned above, such curves derived from analytic expressions of the atmospheric turbulence spectrum and of the Zernike modes constitute an interesting solution for the spectral shaping filters, as they can be

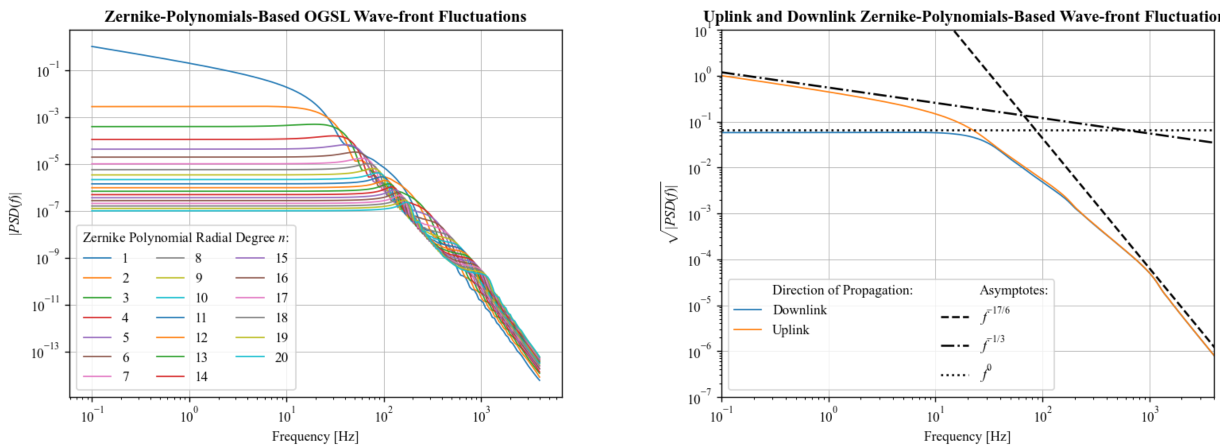

(a) The temporal power spectral densities (PSDs) for each Zernike radial degree are plotted for $1 \leq n \leq 20$. Such curves obtained through the numerical integration of Eq. (5) are normalized with respect to the maximum value of the tip-tilt curve ($n = 1$).

(b) Square root of the temporal PSDs for uplink and downlink turbulence-induced wave-front fluctuations. Downlink is considered affected by scintillation, while uplink is characterised by the joint effect of scintillation and beam wander. The asymptotic behaviour of the curves is highlighted.

Figure 3: Representative curves of the OGSL fades' frequency response. Analytic expressions of the atmospheric turbulence spectrum and of Zernike polynomials were employed.

computed for virtually any OGSL scenario. Nevertheless, the double numerical integration which is required to solve Eq. (5), for each radial degree n, makes the derivation of such analytic filters extremely time consuming, and severely limits the performance of the random vector generation method described in Sec. 3.3.

4.2 A Simplified Model

The idea of using an approximated solution for the filters required in the random vectors generation was already implicitly introduced in previous publications, where generic low-pass filters (LPFs) were employed to apply the desired spectrum.[26] Nevertheless, in such cases the LPFs were not specifically derived for each OGSL scenario, as they were rather defined as simulation inputs. In fact, the filter's characteristics were manually set by the user, in terms of cut-off frequency and curve slope, according to a limited set of available direct channel measurements data. This is certainly a good approach to obtain an initial set of results, however it cannot be adapted to represent link scenarios which differ from those characterising the actual data set, which to our knowledge was not large enough to derive a filter generation model.

Leveraging on the insight provided by the analytical curves derived in Sec. 4.1. and on the comparison with results obtained by the End-to-end Monte Carlo simulations described in Sec. 3.2., in this section a model is proposed for the filters used in the fading vectors spectral shaping process.

Firstly, given their excellent gain response, Butterworth low-pass filters represent a well-suited candidate for the type of LPFs applied in the fading vectors spectral shaping. In fact, such kind of filter presents a constant gain in the spectrum preceding its cut-off frequency, and then decreases its amplitude in a monotonic fashion without displaying ripples or similar unwanted behaviour. In addition, Butterworth filters are commonly used and easily implementable with common software packages.

Secondly, as any low-pass filter, the Butterworth filters which shall approximate the curves in Fig. 3b are defined by two quantities: the cut-off frequency f_c ($[f_c] = Hz$) and the slope, described in dB/decade, which is determined by the filter's order.

For what concerns the first point, it was already noticed that the cut-off frequency of the curves representing the temporal power spectrum of the fading processes is proportional to the atmospheric wind speed profile $V(h)$. When dealing with atmospheric turbulence, a characteristic frequency which is representative of the fades' temporal behaviour is the Greenwood frequency f_G. This parameter, introduced for the design of adaptive optics control systems, is associated with high-order wave-front fluctuations, and can indeed be used to describe the dynamics of the scintillation process. Its expression is given by Eq. (6):[31]

$$f_G = 2.31\lambda^{-6/5}\cos(\zeta)^{-3/5}\left[\int_h C_n^2(h)V(h)^{5/3}\,dh\right]^{3/5} \tag{6}$$

and is used to obtain the representative curves in Fig. 4. One can easily notice how the value of the Greenwood frequency depends not only on the turbulence strength — through $C_n^2(h)$ and $V(h)$ — but also on the link elevation angle $\varepsilon = \pi/2 - \zeta$. In particular, OGSLs performed at lower elevations suffer a scintillation process with a higher rate of change. Moreover, because of the dependence of the wind profile on the satellite slew rate (see Eq. (2)), OGSLs established with terminals on board LEO satellites are characterised by significantly higher f_G values with respect to ground-to-GEO cases.

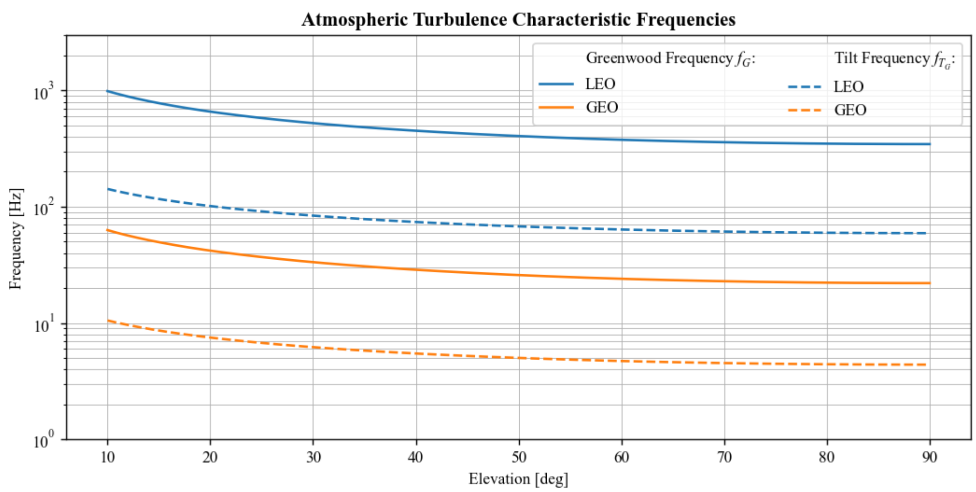

Figure 4: Greenwood and tilt frequencies represented for OGSLs performed with a geostationary and LEO satellite at 1000km of altitude. The values used in Eqs. (6) and (7) to derived f_G and f_{T_G} were a ground wind speed of 6m/s, weak turbulence conditions ($A = 1.7 \cdot 10^{-14} m^{-2/3}$), $D_{\mathrm{Rx}} = 0.25m$ and a signal wavelength of 1550nm.

Similarly to the Greenwood frequency, the tilt frequency f_{T_G} is used to describe the rate of change of the received beam tip-tilt. It can be used to describe the dynamics of the beam wander process, and is defined as:[31]

$$f_{T_G} = 0.331 D_{\mathrm{Rx}}^{-1/6}\lambda^{-1}\cos(\zeta)^{-1/2}\left[\int_h C_n^2(h)V(h)^2\,dh\right]^{1/2} \tag{7}$$

where the dimension of the receiver's aperture diameter D_{Rx} is also included.

Both characteristic frequencies can be used in the definition of the spectral shaping LPFs, with f_G being the cut-off frequency of the Butterworth filter used to represent the scintillation process, and f_{T_G} being the cut-off frequency of the Butterworth filter used to represent the beam wander process experienced in the uplink.

For what concerns the filters' slopes, the analysis of the curves derived analytically have identified a common power law of -17/6 in the high frequency spectrum, with a differentiation of the downlink and uplink channel behaviour in the low frequencies. In the first case, a power law of 0 is observed, while the second case is characterised by a power law of -1/3.

Modelling such behaviour with a Butterworth LPF requires an approximation of the fractional power laws to integer values. This suggests that the filter used in the downlink spectral shaping can be approximated by a Butterworth LPF of third order — which introduces a -30dB/decade slope — with a cut-off frequency equal to f_G. The uplink channel, on the other hand, requires a Butterworth LPF of first order — which introduces a slope of -10dB/decade — with a cut-off frequency equal to f_{T_G}, combined with a second filter in order to represent the high frequency scintillation behaviour. Such second filter must be a Butterworth LPF of second order, with a cut-off frequency equal to the Greenwood frequency. In fact, the combination of the first and second order Butterworth LPFs is such that, even in the uplink case, the curve displays a -30dB/decade gain in the high frequency spectrum.

The conclusions on the model proposed for the spectral shaping filters are summarized in Tab. 2, where the expression $H_{Butter}(f_c, N)$ is representative of a Butterworth filter of cut-off frequency f_c and order N.

Table 2: Butterworth LPFs proposed for the spectral shaping.

Downlink	
Filter $H(f)$	$H_{Butter}(f_G, 3)$
Representative process	Scintillation
Uplink	
Filter $H(f)$	$H_{Butter}(f_{T_G}, 1) \cdot H_{Butter}(f_G, 2)$
Representative process	Beam Wander and Scintillation

Finally, the curves in Fig. 5a and 5b display the comparison between the analytic filters shown in Fig. 3b and those derived from the approximated Butterworth LPF-based model.

One can firstly notice how in both cases the high frequency behaviour displayed by the simplified model practically matches that of the analytic curve, confirming that the -30dB/decade slope is indeed not far from the $f^{-17/6}$ asymptote previously noticed. This also suggests that the third order Butterworth LPF used in the downlink propagation and the combination of the first and second order Butterworth LPFs used in the uplink propagation yield similar high frequency characteristics, as expected.

Secondly, in both cases the Butterworth LPF displays a cut-off frequency slightly higher than the one predicted by the Zernike-polynomials-based filter. This could be due to the difference in which the atmospheric wind speed is treated in the derivation of the two curves. In fact, as opposed to how $V(h)$ is included in Eq. 5, the Butterworth LPFs are directly defined by the characteristic frequencies expressed by Eqs. 6 and 7.

Lastly, for what concerns the uplink spectral shaping, one can see how the two curves display a greater offset than what is observed in the downlink. Nevertheless, this can be explained by the nature of the Kolmogorov spectrum of turbulence used to compute the analytic curve. In fact, by using Eq. 4 in the derivation of the analytic curve, one directly imposes a monotonic decreasing behaviour in the low frequency spectrum of the tip-tilt mode. While this is valid in theory, in practice such a PSD would yield a process with infinite variance. Since this cannot be the case, in practice one must suppose a curve displaying an initial constant behaviour followed by a progressive decrease in gain. Given how the curves have been normalized, such considerations allow to explain the offset between the two curves in Fig. 5b, as well as why the Butterworth LPF is actually a good candidate for the fades practically measured in OGSL uplinks.

5. RESULTS

In this section the filter proposed for the simplified spectral shaping approach is compared to data obtained with the E2EMC simulations described in Sec. 3.2, for a discrete number of OGSL cases.

The four scenarios which are displayed here are representative of both downlink and uplink propagation for two distinct satellite altitudes which are of great interest for ground-to-space FSOC: a GEO satellite and a LEO satellite in circular orbit at 1000km of altitude with respect to ground. The other parameters of interest, such as wavelength, aperture dimensions or OGS altitude are expressed in Tab. 1. In particular, an elevation angle of 40

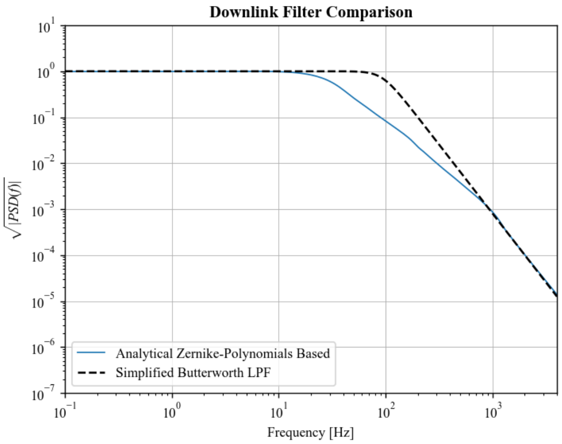

(a) The downlink filter obtained analytically is plotted against the third order Butterworth LPF with cut-off frequency defined by f_G.

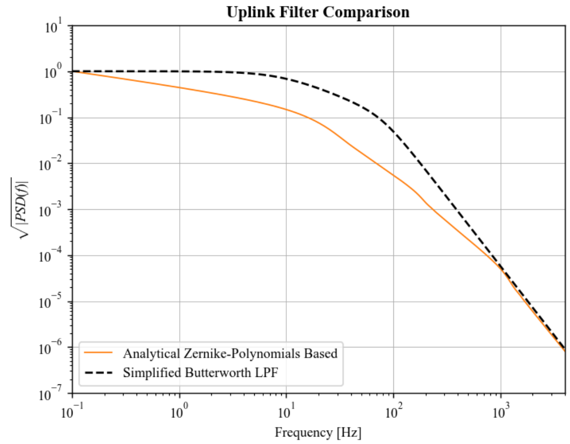

(b) The uplink filter obtained analytically is plotted against the combination of a first and second order Butterworth LPF, defined respectively by f_{T_G} and f_G.

Figure 5: The Zernike-polynomials-based filters derived analytically are compared to those based on the Butterworth low pass filters, obtained for the same link conditions. The curves are normalized to their maximum values.

degrees was chosen as it is what generally characterises GEO OGSLs performed in Europe. The same elevation angle was kept also for the LEO OGSLs simulations in order to visualize the impact of the different satellite altitude on the received signal temporal power spectrum.

For each analysed case a periodogram was performed on the simulated power vector time series in order to derive its PSD. Successively, according to the propagation channel, for the same link characteristics the frequencies f_G and f_{T_G} were computed and used to derive the Butterworth LPF as specified in Tab. 2. As shown in Fig. 6, 7, 8 and 9, such filters were finally plotted against the square root of the simulated PSDs in order to derive a qualitative performance of the spectral shaping filters obtained applying the method proposed in this work.

Observing Fig. 6 one can notice the good agreement there is between the two curves. The asymptotic behaviour in the high frequency spectrum is respected by the Butterworth LPF, and its cut-off frequency is in the near proximity of the one characterising the simulated data PSD. On the contrary, the cut-off frequency predicted by the simplified model for the LEO downlink (see Fig. 7) is greater than what is displayed by the simulated data. This phenomenon, which was also highlighted in the description of Fig. 5a, supports the idea according to which such offset may be due to the different manner in which the contribution of the wind profile is handled in the determination of the Zernike-polynomials-based curves and in the Greenwood frequency which determines the Butterworth filter gain. In particular, since the offset is especially visible in the LEO-to-ground case, where the satellite speed with respect to ground is high, a valid hypothesis is that in this case the apparent wind speed contribution caused by the satellite motion in Eq. 2 may be overestimated.

For what concerns the uplink cases, both Fig. 8 and 9 display a good agreement between the Butterworth LPFs and the simulated curves. The combination of the first and second order Butterworth filters allows to reproduce the gradual decrease in gain which is observed for frequencies greater than the tilt frequency f_{T_G}. This supports the considerations developed in Sec. 4.2 concerning the difference between what is predicted mathematically by the Kolmogorov power-law spectrum and what is practically observed. Furthermore, the -30dB/decade slope in the high frequencies aligns well with the simulated PSDs' asymptotic behaviour.

In all the cases presented, the PSDs obtained from the E2EMC simulations display the typical ripples which are predicted from the theoretical model based on the Zernike polynomials temporal power spectrum, as opposed to the Butterworth LPFs. Nevertheless, despite their approximated behaviour, the latter approach which

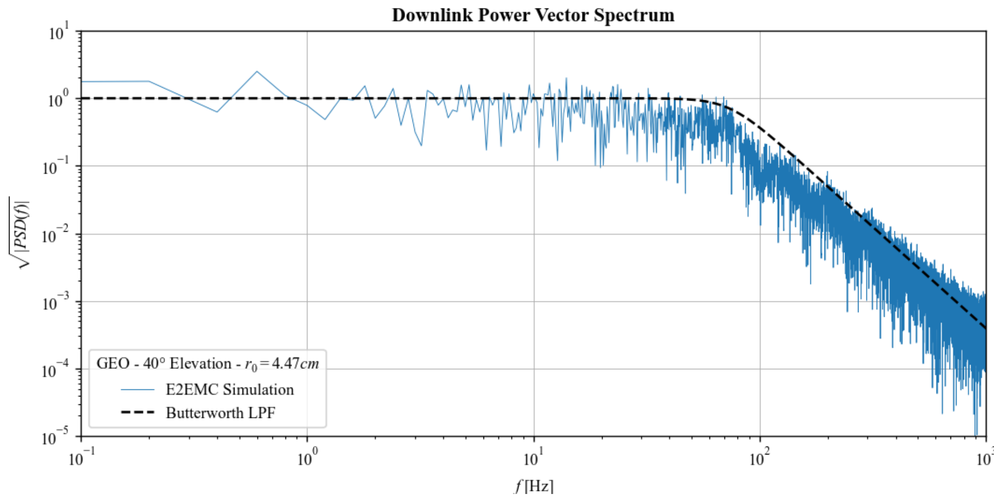

Figure 6: Received optical power vector spectrum for a GEO-to-ground link. The Butterworth LPF is compared to the square root of the PSD obtained from the E2EMC simulation. In both cases the turbulence strength is defined by the Fried parameter $r_0 = 4.47$cm.

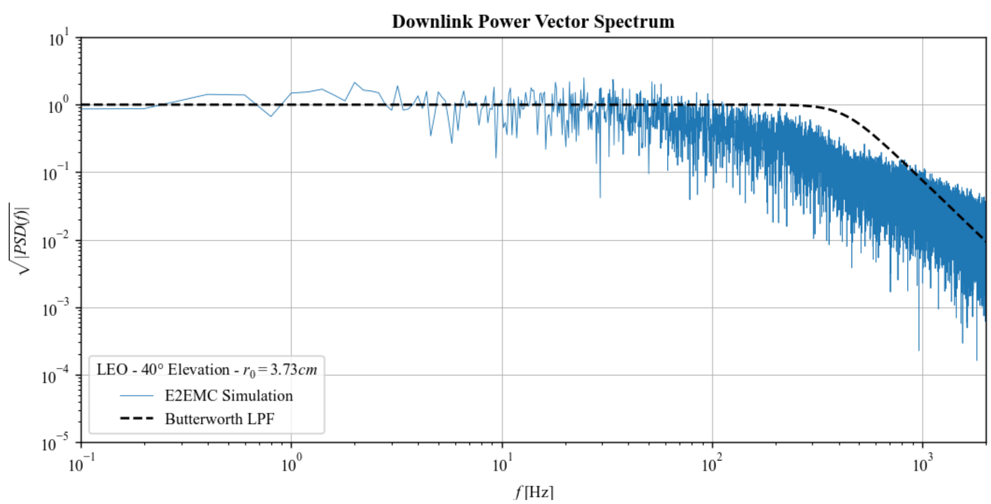

Figure 7: Received optical power vector spectrum for a LEO-to-ground link. The Butterworth LPF is compared to the square root of the PSD obtained from the E2EMC simulation. In both cases the turbulence strength is defined by the Fried parameter $r_0 = 3.73$cm.

has been presented in this work constitutes an efficient alternative which can be implemented in the spectral generation to obtain representative power vectors for virtually any scenario of interest, given their dependence on characteristic frequencies which can be easily computed. Fig. 10a and 10b provide an example of the output which can be obtained. In particular, the Butterworth LPF displayed in Fig. 6 was used in the vector generation algorithm described in Sec. 3.3 in order to shape the spectrum of a previously generated Gaussian vector. Successively, a non-linear transformation was applied in order to modify the vector's statistics in accordance with the scintillation index analytically derived for the particular OGSL scenario.

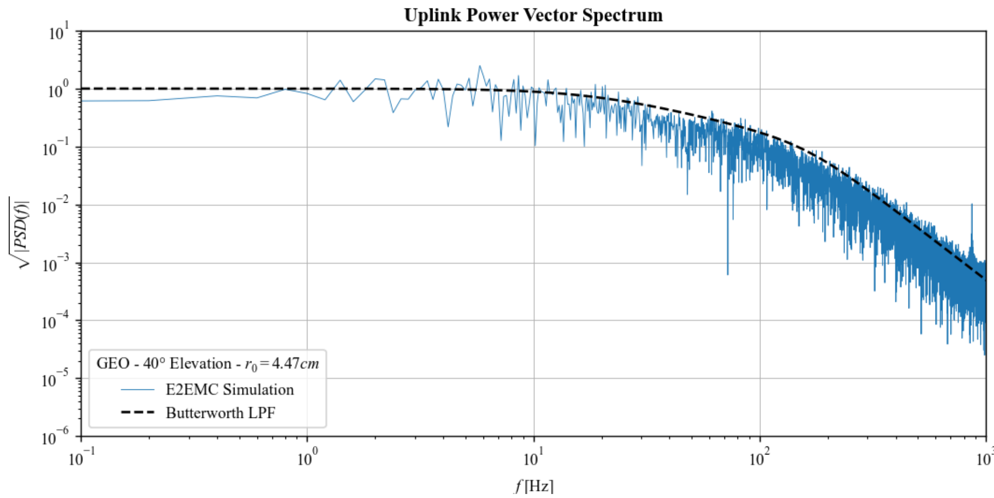

Figure 8: Received optical power vector spectrum for a ground-to-GEO link. The Butterworth LPF is compared to the square root of the PSD obtained from the E2EMC simulation. In both cases the turbulence strength is defined by the Fried parameter $r_0 = 4.47$cm.

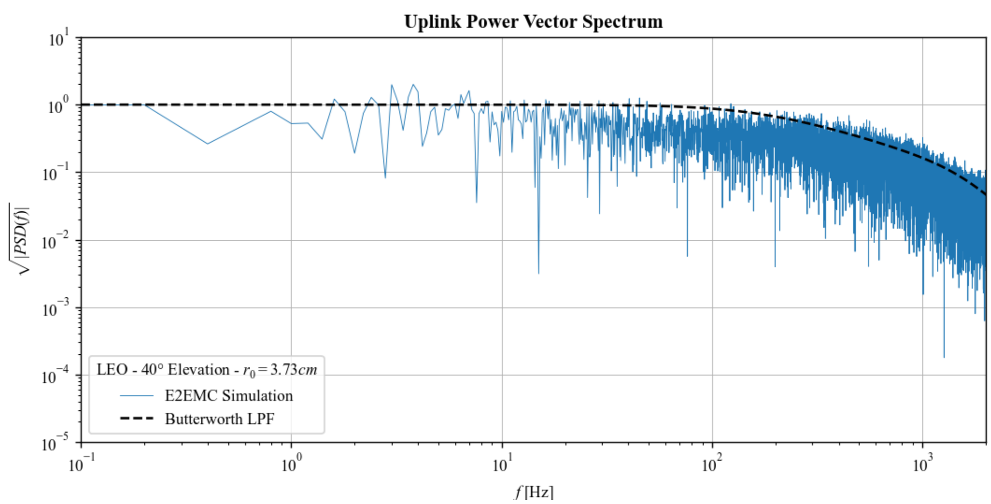

Figure 9: Received optical power vector spectrum for a ground-to-LEO link. The Butterworth LPF is compared to the square root of the PSD obtained from the E2EMC simulation. In both cases the turbulence strength is defined by the Fried parameter $r_0 = 3.73$cm.

6. CONCLUSION AND FUTURE WORK

The presented simplified spectral shaping approach models the turbulent atmosphere dynamics of optical power in both uplink and downlink optical satellite links and can be used to generate realistic signal dynamics at the received side considering terminal and link geometry and atmospheric parameters. The method is based on the generation of a Butterworth filter defined by a cut-off frequency which is computed for every scenario of interest, and a slope which is characteristic of the channel in the given link direction. The model was also validated against data obtained with an experimentally validated simulation tool. Its computation is not only tailored to the optical feeder-link configuration, but is also extremely time efficient, hence represents an ideal solution to be implemented, for example, in network wide simulations.

The work presents an extensive explanation of the filter parameter derivation that can be used for virtually

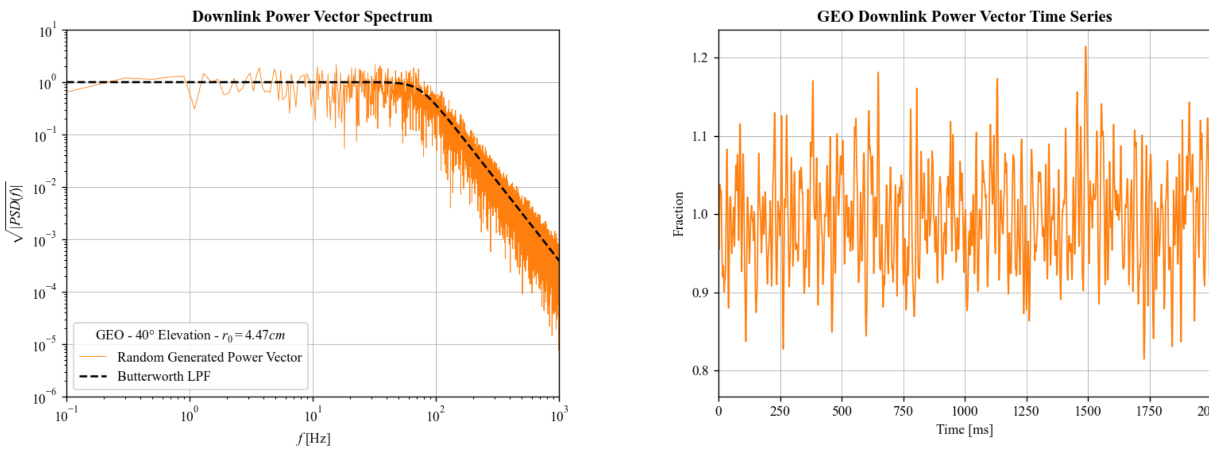

(a) Temporal power spectrum of the generated power vector after spectral shaping.

(b) 2 seconds time series of the received optical power vector, normalized with respect to its mean.

Figure 10: Practical example of how the Butterworth LPF can be used to generate a realistic time series of received optical power for an OGSL. The signal dynamics are determined by the spectral shaping process.

any optical link scenario and application. Furthermore, considering realistic transmitter characteristics such as transmitted power, an absolute optical power vector can be generated. If also the optical receiver implementation characteristics are known, such as sensitivity, noises and resynchronisation times, then time-dependent fading vectors can be obtained as well. This allows for an analysis of coding performance during the design phase.

Future work will include the modelling of the impact of an optical system implementation, including adaptive optics and fibre-coupling. Also, advancements in the state-of-the-art of the apparent wind speed due to the satellite slew rate shall be considered with the objective of a unified channel and system model for link budget analysis, signal dynamics prediction and power vector generation.

Acknowledgement

The authors would like to acknowledge the discussions and the support of the European Space Agency (ESA) under the Project "HydRON Simulator Testbed", Contract No. ESA AO/1-10623/21/NL/CLP. The views of the authors do not reflect the views of the Agency.

REFERENCES

[1] Calvo, R. M., Poliak, J., Surof, J., Reeves, A., Richerzhagen, M., Kelemu, H. F., Barrios, R., Carrizo, C., Wolf, R., Rein, F., Dochhan, A., Saucke, K., and Luetke, W., "Optical technologies for very high throughput satellite communications," in [*Free-Space Laser Communications XXXI*], Hemmati, H. and Boroson, D. M., eds., **10910**, 109100W, International Society for Optics and Photonics, SPIE (2019).

[2] European Space Agency (ESA), *ESA SPECIFICATION FOR TERABIT/SEC OPTICAL LINKS (ESTOL)* (07 2023). Rev. 1.0.

[3] Giggenbach, D., Shrestha, A., Moll, F., Fuchs, C., and Saucke, K., "Reference power vectors for the optical leo downlink channel," in [*2019 IEEE International Conference on Space Optical Systems and Applications (ICSOS)*], 1–4, IEEE (2019).

[4] Andrews, L. and Phillips, R., "Laser beam propagation through random media (bellingham, washington," (2005).

[5] Giggenbach, D. and Shrestha, A., "Atmospheric absorption and scattering impact on optical satellite-ground links," *International Journal of Satellite Communications and Networking* **40**(2), 157–176 (2022).

[6] Giggenbach, D., Moll, F., Fuchs, C., de Cola, T., and Mata-Calvo, R., "Space communications protocols for future optical satellite-downlinks," (2011).

[7] Andrews, L. C., [*Field guide to atmospheric optics*] (2019).

[8] Bian, Y., Li, Y., Chen, E., Li, W., Hong, X., Qiu, J., and Wu, J., "Free-space to single-mode fiber coupling efficiency with optical system aberration and fiber positioning error under atmospheric turbulence," *Journal of Optics* **24**(2), 025703 (2022).

[9] Carrasco-Casado, A. and Mata-Calvo, R., "Space optical links for communication networks," in [*Springer Handbook of Optical Networks*], 1057–1103, Springer (2020).

[10] Kiesaleh, K. and Yan, T.-Y., "A statistical model for evaluating gopex uplink performance," *The Telecommunications and Data Acquisition* (1992).

[11] Giggenbach, D., Moll, F., and Perlot, N., "Optical communication experiments at dlr," *Journal of the National Institute of Information and Communications Technology* **59**(1.2), 125–134 (2012).

[12] Perlot, N., Knapek, M., Giggenbach, D., Horwath, J., Brechtelsbauer, M., Takayama, Y., and Jono, T., "Results of the optical downlink experiment kiodo from oicets satellite to optical ground station oberpfaffenhofen (ogs-op)," in [*Free-Space Laser Communication Technologies XIX and Atmospheric Propagation of Electromagnetic Waves*], **6457**, 28–35, SPIE (2007).

[13] Toyoshima, M., Takahashi, T., Suzuki, K., Kimura, S., Takizawa, K., Kuri, T., Klaus, W., Toyoda, M., Kunimori, H., Jono, T., et al., "Laser beam propagation in ground-to-oicets laser communication experiments," in [*Atmospheric Propagation IV*], **6551**, 104–115, SPIE (2007).

[14] Hristovski, I. R., Campelo, A. R., Femenía-Castella, B., Doensdorf-Sternal, E., Duliu, A. O., Haeusler, S., Holzman, J. F., Klemich, K., Laidlaw, D. J., Marynowski, T., et al., "Pre-distortion adaptive optics: experimental results from bi-directional tracking links between dlr's optical ground station and alphasat's tdp-1 terminal," in [*Free-Space Laser Communications XXXVI*], **12877**, 328–336, SPIE (2024).

[15] Ratcliffe, J. A., "Some aspects of diffraction theory and their application to the ionosphere," *Reports on progress in physics* **19**(1), 188 (1956).

[16] Mercier, R., "Diffraction by a screen causing large random phase fluctuations," in [*Mathematical Proceedings of the Cambridge Philosophical Society*], **58**(2), 382–400, Cambridge University Press (1962).

[17] Lee, R. W. and Harp, J. C., "Weak scattering in random media, with applications to remote probing," *Proceedings of the IEEE* **57**(4), 375–406 (1969).

[18] Liu, Y.-B. and Wu, R.-S., "A comparison between phase screen, finite difference, and eigenfunction expansion calculations for scalar waves in inhomogeneous media," *Bulletin of the seismological society of America* **84**(4), 1154–1168 (1994).

[19] Fusco, T., Conan, J.-M., Michau, V., Mugnier, L., and Rousset, G., "Efficient phase estimation for large-field-of-view adaptive optics," *Optics letters* **24**(21), 1472–1474 (1999).

[20] Osborn, J., Townson, M. J., Farley, O. J., Reeves, A., and Calvo, R. M., "Adaptive optics pre-compensated laser uplink to leo and geo," *Optics Express* **29**(4), 6113–6132 (2021).

[21] Hristovski, I. R., Osborn, J., Farley, O. J., Townson, M. J., Calvo, R. M., Femenía-Castella, B., Torres, J. S., Holzman, J. F., and Reeves, A. P., "Pre-distortion adaptive optics for optical feeder links: simulations and performance analyses," *Optics Express* **32**(12), 20976–20991 (2024).

[22] Schmidt, J., [*Numerical Simulation of Optical Wave Propagation with Examples in MATLAB*], Press monograph, SPIE (2010).

[23] Gujar, U. and Kavanagh, R., "Generation of random signals with specified probability density functions and power density spectra," *IEEE Transactions on Automatic Control* **13**(6), 716–719 (1968).

[24] Kiasaleh, K., "On the probability density function of signal intensity in free-space optical communications systems impaired by pointing jitter and turbulence," *Optical Engineering* **33**(11), 3748–3757 (1994).

[25] Toyoshima, M., Yamakawa, S., Yamawaki, T., Arai, K., García-Talavera, M. R., Alonso, A., Sodnik, Z., and Demelenne, B., "Long-term statistics of laser beam propagation in an optical ground-to-geostationary satellite communications link," *IEEE transactions on antennas and propagation* **53**(2), 842–850 (2005).

[26] Giggenbach, D., Parthasarathy, S., Shrestha, A., Moll, F., and Mata-Calvo, R., "Power vector generation tool for free-space optical links—pvget," in [*2017 IEEE International Conference on Space Optical Systems and Applications (ICSOS)*], 160–165, IEEE (2017).

[27] Carrillo-Flores, A., Giggenbach, D., Shrestha, A., and Knopp, M. T., "Absolute power vectors for the optical leo uplink channel," in [*COAT2023*], (2023).

[28] Noll, R. J., "Zernike polynomials and atmospheric turbulence," *JOsA* **66**(3), 207–211 (1976).

[29] Liu, C., Chen, S., Li, X., and Xian, H., "Performance evaluation of adaptive optics for atmospheric coherent laser communications," *Optics express* **22**(13), 15554–15563 (2014).

[30] Conan, J.-M., Rousset, G., and Madec, P.-Y., "Wave-front temporal spectra in high-resolution imaging through turbulence," *JOSA A* **12**(7), 1559–1570 (1995).

[31] Tyler, G. A., "Bandwidth considerations for tracking through turbulence," *JOSA A* **11**(1), 358–367 (1994).